Quantifying Balance Capabilities for Optimal Mechanism Design

Brandon J. DeHart, Rob Gorbet, and Dana Kulić

Abstract— **For legged systems, achieving balance and locomotion depends on the system's capability to effectively and efficiently move its Center of Mass relative to its contact point(s). To measure this capability, we introduce a generalization of velocity gains: dynamic ratios which quantify this motion for passive contacts. We incorporate this generalized gain into an objective function and apply weighted matrix norms to facilitate the parameterized design optimization of 3D mechanisms. We then demonstrate the proposed approach in the design of a 3D 5-link biped across several different design objectives.**

I. Introduction

The two most important behaviors for legged systems are balance and locomotion. Both behaviors are directly related to a system's overall dynamics and therefore both improve if the system is more effective at moving its Center of Mass (COM) relative to its contact point(s):

- When balancing, a legged system attempts to maintain its COM above the area defined by its contact point(s), only changing its contact point(s) when necessary.
- During locomotion (or gait), a legged system moves itself, and by extension its COM, by pushing against a set of periodically changing contact point(s).

Whether the system is standing still or walking, external disturbances may require real-time adjustments to its COM motion. In all cases, a legged system that is able to more effectively move its COM will also be more effective when balancing, walking, and compensating for disturbances.

The capacity of a legged system to move its COM relative to its contact point(s) depends on both the controller used to perform the motion and the physical properties of the system. Although much work has been done to date on how to develop controllers which can realize balance and gait tasks for legged systems, only limited research has investigated the quantification of a system's physical capabilities or how to adjust the system's design to improve them.

The two main existing measures of a mechanism's inherent balance abilities are dynamic COM manipulability [1]–[3] and velocity and momentum gains [4]–[8]: Dynamic COM manipulability generates an ellipsoid in 3D space which approximates a system's COM acceleration limits, while velocity and momentum gains are defined as a set of dynamic ratios which quantify how quickly an articulated system can move its COM while balancing on a passive contact.

*This work was supported by the Natural Sciences and Engineering Research Council of Canada (NSERC).

Brandon J. DeHart and Dana Kulić are with the Department of Electrical & Computer Engineering, University of Waterloo, Ontario, Canada.

Rob Gorbet is with the Department of Knowledge Integration, University of Waterloo, Ontario, Canada.

{bjdehart,rbgorbet,dana.kulic}@uwaterloo.ca

In [7], we extended Featherstone's initial momentum gain definitions for a planar 2-link mechanism (as defined in [6]) to general 2D and 3D systems. We then demonstrated and compared velocity and momentum gains as objective metrics for mechanism optimization using a novel optimization framework, for simple planar balancing systems.

Based on the results of this gain comparison, we used angular momentum gain as the objective in optimizing the design of a 5-link planar biped and compared the results to optimizing the same mechanism using a cost of transport based objective function in [8]. We showed that these two objectives produced very similar results, even though the angular momentum gain calculation requires only the joint space inertia matrix at each configuration of interest while the cost of transport calculation requires slow hybrid dynamics equations and pre-generated or co-optimized trajectories.

In this paper, we develop a general framework for characterizing a system's ability to move its COM and for optimizing its design based on this metric, building on the existing velocity and momentum gain research in [4]–[8] by

- Defining a generalized gain, and showing that all of the existing velocity and momentum gains are special cases and/or subsets of this general gain.
- Formulating an optimization framework using this generalized gain in tandem with weighted matrix norms to enable the application of domain knowledge.
- Validating this generalized optimization framework with the optimized design of a 3D bipedal mechanism.

After outlining the related work below, we provide a brief review of velocity and momentum gains in Section II. We then define the generalized gain equation in Section III and show that it can be used to formulate all of the existing gains. We also use this generalized gain formulation to directly show that the differences between velocity and momentum gains are entirely a function of scaling.

Following these definitions, we formulate our optimization framework in Section IV with a novel generalized objective function using weighted matrix norms and the new generalized gain from Section III. We then validate the generalized optimization framework in Section V by applying 1-, 2-, and ∞-norms along with 2 different types of weighting matrices to the optimization of a 3D 5-link biped model.

Finally, we discuss these results, the framework, and the generalized gains in Section VII before summarizing and providing directions for future work in Section VIII.

A. Related Work

Several prior works investigate the possibility of generating dynamic biped parameters using optimization [9]–[15].

In these works, either the cost of transport or the number of steps is used as the optimization metric, with a dual objective of both gait generation and physical property selection.

Genetic algorithms and evolutionary computing were used in [9], [10] to select control parameters (or, equivalently, a trajectory) and generate dynamic parameters in parallel. This was one of the first examples of the generation of physical properties for bipeds using optimization.

Later, Haberland *et al.* developed a generic framework for extracting design principles from observed biological systems [11], [12] . Using the biological observations, a non-dimensionalized design space is populated with principles and then sampled. Optimal control is then used to test whether the principle is valid for the given design space.

In [13], an optimization is developed using a single design parameter, the spring constant between the model's legs, to optimize the design parameters and generate gait. The system is then controlled using trajectory tracking by reducing the biped to a 1 DOF system using hybrid zero dynamics [16].

Another framework was developed in [14], which used simulation to co-optimize the control and design of bipeds. Comparing this recent work to the original methods found in [9], [10], the key differences are the addition of full 2D and 3D dynamics in a simulated environment and the possibility of non-periodic gait. Building on this approach, [15] fixed the robot's dynamic parameters and optimized the spring constants and trajectories (state and input) to design compliant gait trajectories for bipeds. We also use a passive rotational joint in place of the stance ankle and ignore the instantaneous dynamics of stepping, as proposed in [15].

The above works all use a controller, either pre-existing or co-optimized, as part of the formulation of their dynamic parameter optimization. Therefore, the mechanisms which are found are optimized only for the given controller. The objective functions of these optimizations are all based on the cost of transport, with several also using torque norms for comparison. These measures are both dependent on the trajectory and/or controller which is applied.

Although this approach has shown successful results, it limits the prospective applications of the biped to those which were conceived as part of the optimization and can suffer from overfitting (to the controller, trajectory, or both). It also assumes that a controller must be developed (or at least parameterized) either prior to or as part of the overall parameterization of the biped. This limits these methods to a specific controller, or subset of controllers, which prevents general applicability of the biped itself for other use cases.

To avoid these issues, some researchers have focused on how to quantify a mechanism's inherent balancing capabilities, or how to modify the mechanism to improve these capabilities, without depending on (and potentially overfitting to) a particular controller and/or trajectory formulation.

Building on earlier work ([1], [2]), Azad *et al.* proposed a formulation of dynamic COM manipulability in [3], which defines a system's physical COM acceleration limits as an ellipsoid. However, this metric depends on the specification of a weighting matrix for normalization and the ellipsoid that is generated must be projected into lower dimensions to be used for balance. Dynamic COM manipulability has been successfully used to optimize a postural task for the iCub robot as part of the CoDyCo project [17].

An alternative metric was proposed by Featherstone in [4] and extended in [5], [6]: A set of dynamic ratios he called velocity gains, which quantify how fast an articulated system balancing on a passive contact can move its COM. These velocity gains are independent of the control scheme used, as they are functions only of the properties and configuration of the mechanism, and provide an upper bound on how well any controller could balance the given mechanism[1]. Velocity gains were also recently successfully used in the development of effective planar balance controllers [18]–[20].

Featherstone also defined momentum gains for 2-link planar systems in [6], which we extended to general 2D and 3D systems in [7] and then applied to the optimization of a 2D 5-link biped in [8]. In the next section we will briefly review the existing work on velocity and momentum gains, including our simplified notation, before developing our proposed generalized gain metric in Section III.

II. Velocity and Momentum Gains: A Review

Velocity and momentum gains quantify how fast an articulating system balancing on a passive (possibly rolling) contact can move its COM. In addition to their independence from the controller and/or trajectory used, these gains are invariant to a scaling of the total mass of the system, and the angular gains are also invariant to a scaling of total length, allowing the balancing capabilities of an entire class of mechanisms to be quantified with a single metric [6].

In this section, we will briefly review the general (2D and 3D) velocity and momentum gains defined in [6]–[8], including the development of augmented inertia matrix notation and a formulation for relating the general 3D gains to the system's centroidal momentum via a spatial gain.

A. Velocity Gains

Linear velocity gain [6] is defined as a ratio of the change in horizontal COM velocity relative to an impulsive change in the velocity of the model's actuated joint(s), assuming a single passive (rolling or point) contact with the environment.

Similarly, angular velocity gain [6] is defined as a ratio of the change in angular COM velocity about the (instantaneous, if rolling) contact point relative to an impulsive change in the velocity of the model's actuated joint(s).

For 3D models, the linear velocity gain $\boldsymbol{G}_v$ includes both horizontal directions of motion, while the angular velocity gain $\boldsymbol{G}_\omega$ includes all 3 rotations[2] about the contact point:

$$\boldsymbol{G}_v(\Delta\dot{\boldsymbol{q}}_a) = \begin{bmatrix}\Delta\dot{c}_x\\ \Delta\dot{c}_y\end{bmatrix} \quad \boldsymbol{G}_\omega(\Delta\dot{\boldsymbol{q}}_a) = \Delta\dot{\phi} = \frac{\boldsymbol{c}\times\Delta\dot{\boldsymbol{c}}}{c^2} \quad (1)$$

[1]In this context, balance is assumed to be primarily a function of COM motion. Angular momentum about the COM is assumed to be regulated.

[2]Although the $\boldsymbol{G}_\omega$ component about the vertical axis does not contribute to balance, it was included in the original definition of $\boldsymbol{G}_\omega$ along with a brief discussion of how it could be used in spinning motions [6].

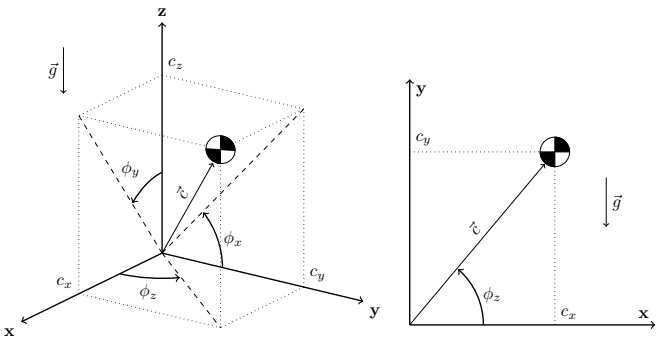

(a) 3D Coordinates (b) 2D Coordinates

Fig. 1. In general, $\boldsymbol{c} = [c_x\ c_y\ c_z]^T$ is a vector from the contact point to the COM and the angles $\boldsymbol{\phi} = [\phi_x\ \phi_y\ \phi_z]^T$ are measured from the reference frame to $\boldsymbol{c}$. For 2D, we assume gravity acts in the $-\mathbf{y}$ direction and $c_z = 0$.

where $\boldsymbol{c} = [c_x\ c_y\ c_z]^T$ is a vector from the contact point to the COM with length $c = \|\boldsymbol{c}\|_2$, the change in COM velocity is $\Delta\dot{\boldsymbol{c}} = [\Delta\dot{c}_x\ \Delta\dot{c}_y\ \Delta\dot{c}_z]^T$, the change in angular COM velocity about the contact point is $\Delta\dot{\boldsymbol{\phi}} = [\Delta\dot{\phi}_x\ \Delta\dot{\phi}_y\ \Delta\dot{\phi}_z]^T = (\boldsymbol{c}\times\Delta\dot{\boldsymbol{c}})/c^2$, and the change in actuated joint velocity is $\Delta\dot{\boldsymbol{q}}_a$ (see Figure 1a). Note that in these equations, it is assumed that $\Delta\dot{\boldsymbol{q}}_a$ is a unit velocity step (i.e., $\|\Delta\dot{\boldsymbol{q}}_a\| = 1$) [6]. Both gains are divided by the velocity step magnitude, which gives $\boldsymbol{G}_v$ units of length and makes $\boldsymbol{G}_\omega$ dimensionless.

For a planar model, we assume that gravity acts in the $-\mathbf{y}$ direction and set $c_z = 0$, resulting in $\boldsymbol{\phi} = [0\ 0\ \phi_z]^T$ (see Figure 1b). Using this to simplify Equation (1), we can extract the scalar velocity gains defined in [6] for planar models: $G_v(\Delta\dot{\boldsymbol{q}}_a) = \Delta\dot{c}_x$ and $G_\omega(\Delta\dot{\boldsymbol{q}}_a) = \Delta\dot{\phi}_z$.

When using the Augmented Inertia Matrix method [6] to calculate the velocity gains, virtual immobile prismatic joints (labeled $0 = \{x, y, z\}$) are inserted between the passive contact and the inertial reference frame. The impulsive dynamics, with these 3 virtual prismatic joints (labeled 0) and 3 passive rotational joints (labeled p) at the contact, and the actuated joints (labeled a), are therefore:

$$\mathbf{H}'\Delta\dot{\boldsymbol{q}}' = \begin{bmatrix} \mathbf{H}_{00} & \mathbf{H}_{0p} & \mathbf{H}_{0a} \\ \mathbf{H}_{p0} & \mathbf{H}_{pp} & \mathbf{H}_{pa} \\ \mathbf{H}_{a0} & \mathbf{H}_{ap} & \mathbf{H}_{aa} \end{bmatrix} \begin{bmatrix} 0 \\ \Delta\dot{\boldsymbol{q}}_p \\ \Delta\dot{\boldsymbol{q}}_a \end{bmatrix} = \begin{bmatrix} \boldsymbol{\iota}_0 \\ 0 \\ \boldsymbol{\iota}_a \end{bmatrix} \quad (2)$$

where $\boldsymbol{\iota}_0$ and $\boldsymbol{\iota}_a$ are virtual joint and actuated joint impulses, respectively, and $\mathbf{H}'$ is the Augmented Joint Space Inertia Matrix[3]. This enables the direct calculation of $\Delta\dot{\boldsymbol{c}}$ since the virtual impulse $\boldsymbol{\iota}_0 = m\Delta\dot{\boldsymbol{c}}$, where m is the total mass [6].

Since $\mathbf{H}_{pp}$ is a 3x3 symmetric positive definite matrix, we can use the middle row to get $\Delta\dot{\boldsymbol{q}}_p = -\mathbf{H}_{pp}^{-1}\mathbf{H}_{pa}\Delta\dot{\boldsymbol{q}}_a$ [6], and the equation for $\Delta\dot{\boldsymbol{c}}$ can be written as:

$$\Delta\dot{\boldsymbol{c}} = \frac{1}{m}\left(\mathbf{H}_{0a} - \mathbf{H}_{0p}\mathbf{H}_{pp}^{-1}\mathbf{H}_{pa}\right)\Delta\dot{\boldsymbol{q}}_a \quad (3)$$

In 2D, with only one passive contact joint (i.e., $p = \{1\}$), $\mathbf{H}_{pp}$ is a scalar and we get $\mathbf{H}_{pp}^{-1} = H_{11}^{-1} = 1/H_{11}$.

[3]The standard Joint Space Inertia Matrix $\mathbf{H}$ is simply the submatrix of $\mathbf{H}'$ where all elements with a 0 in the subscript have been removed.

In any given configuration, the matrix $\mathbf{H}'$ and vector $\boldsymbol{c}$ are fixed. Since the velocity gain equations are linear with respect to $\Delta\dot{\boldsymbol{q}}_a$, we define gain matrices $\mathbf{G}_{*a}$ such that $\boldsymbol{G}_v(\Delta\dot{\boldsymbol{q}}_a) = \mathbf{G}_{va}\Delta\dot{\boldsymbol{q}}_a$ and $\boldsymbol{G}_\omega(\Delta\dot{\boldsymbol{q}}_a) = \mathbf{G}_{\omega a}\Delta\dot{\boldsymbol{q}}_a$ [6]:

$$\begin{aligned} \mathbf{G}_{va} &= \frac{1}{m}\begin{bmatrix} \boldsymbol{H}_{xa} - \boldsymbol{H}_{xp}\mathbf{H}_{pp}^{-1}\mathbf{H}_{pa} \\ \boldsymbol{H}_{ya} - \boldsymbol{H}_{yp}\mathbf{H}_{pp}^{-1}\mathbf{H}_{pa} \end{bmatrix} \\ \mathbf{G}_{\omega a} &= \frac{[\boldsymbol{c}\times]}{mc^2}\left(\mathbf{H}_{0a} - \mathbf{H}_{0p}\mathbf{H}_{pp}^{-1}\mathbf{H}_{pa}\right) \end{aligned} \quad (4)$$

where $[\boldsymbol{c}\times]$ represents the 3x3 skew symmetric matrix.

For 2D systems, the first row of $\mathbf{G}_{va}$ is equivalent to the linear velocity gain vector $\boldsymbol{G}_{va}$, and the third (last) row of $\mathbf{G}_{\omega a}$ is equivalent to the angular gain vector $\boldsymbol{G}_{\omega a}$ [6].

B. Momentum Gains

Momentum gains are defined in a similar way to velocity gains, where the COM velocity is replaced by the COM momentum and impulsive changes in joint velocities are replaced with joint impulses [6]. The general linear ($\boldsymbol{G}_m$) and angular ($\boldsymbol{G}_o$) momentum gains are defined as [7]:

$$\boldsymbol{G}_m(\boldsymbol{\iota}_a) = \begin{bmatrix} \Delta l_x \\ \Delta l_y \end{bmatrix} \quad \boldsymbol{G}_o(\boldsymbol{\iota}_a) = mc^2\Delta\dot{\boldsymbol{\phi}} = \boldsymbol{c}\times\Delta\boldsymbol{l} \quad (5)$$

where $\Delta\boldsymbol{l} = m\Delta\dot{\boldsymbol{c}}$ is the change in linear COM momentum.

In 2D, these reduce to scalar linear and angular momentum gains, giving $G_m(\boldsymbol{\iota}_a) = \Delta l_x$ and $G_o(\boldsymbol{\iota}_a) = mc^2\Delta\dot{\phi}_z$.

The actuator impulse vector (i.e., the instantaneous change in torque $\boldsymbol{\iota}_a = \Delta\boldsymbol{\tau}_a$) is assumed to be a unit step impulse ($\|\boldsymbol{\iota}_a\| = 1$). After dividing the gains by the step impulse magnitude, this means that $\boldsymbol{G}_m$ has units of reciprocal length and makes $\boldsymbol{G}_o$ dimensionless.

There are two key differences between the momentum gains in (5) and the velocity gains in (1) [7]:

- Angular momentum gain ($\boldsymbol{G}_o$) is always finite, while the angular velocity gain ($\boldsymbol{G}_\omega$) approaches infinity as c approaches 0 and is undefined at $c = 0$.
- Momentum gains ($\boldsymbol{G}_m$ and $\boldsymbol{G}_o$) are impulse based, so they inherently incorporate inertial information.

C. H-Bar Notation

To simplify the formulation of impulsive dynamics equations which include an initial passive joint, an augmented joint space inertia matrix notation ($\bar{\mathbf{H}}$) was defined in [7].

The $\bar{\mathbf{H}}$ notation is used to denote the relationship between an impulse and the associated change in joint velocities (i.e., to write $\boldsymbol{\iota}_0 = \bar{\mathbf{H}}_{0a}\Delta\dot{\boldsymbol{q}}_a$ or $\boldsymbol{\iota}_a = \bar{\mathbf{H}}_{aa}\Delta\dot{\boldsymbol{q}}_a$) [7]:

$$\bar{\mathbf{H}}_{\beta\alpha} = \mathbf{H}_{\beta\alpha} - \mathbf{H}_{\beta p}\mathbf{H}_{pp}^{-1}\mathbf{H}_{p\alpha} \quad (6)$$

where α and β can each be either a single joint index or a range of indices provided $\alpha \subset a$. As stated above, for a planar system (where $p = \{1\}$), we know $\mathbf{H}_{pp}^{-1} = 1/H_{11}$.

This allows us to simplify the notation for the impulsive change in COM velocity (due to $\Delta\dot{\boldsymbol{q}}_a$) to

$$\Delta\dot{\boldsymbol{c}} = \frac{1}{m}\left(\mathbf{H}_{0a} - \mathbf{H}_{0p}\mathbf{H}_{pp}^{-1}\mathbf{H}_{pa}\right)\Delta\dot{\boldsymbol{q}}_a = \frac{1}{m}\bar{\mathbf{H}}_{0a}\Delta\dot{\boldsymbol{q}}_a \quad (7)$$

which then also simplifies the velocity gain matrices to

$$\begin{aligned}\mathbf{G}_{va} &= \frac{1}{m}\begin{bmatrix}\boldsymbol{H}_{xa} - \boldsymbol{H}_{xp}\mathbf{H}_{pp}^{-1}\mathbf{H}_{pa}\\ \boldsymbol{H}_{ya} - \boldsymbol{H}_{yp}\mathbf{H}_{pp}^{-1}\mathbf{H}_{pa}\end{bmatrix} = \frac{1}{m}\begin{bmatrix}\bar{\boldsymbol{H}}_{xa}\\ \bar{\boldsymbol{H}}_{ya}\end{bmatrix}\\ \mathbf{G}_{\omega a} &= \frac{[\boldsymbol{c}\times]}{mc^2}\left(\mathbf{H}_{0a} - \mathbf{H}_{0p}\mathbf{H}_{pp}^{-1}\mathbf{H}_{pa}\right) = \frac{[\boldsymbol{c}\times]}{mc^2}\bar{\mathbf{H}}_{0a}\end{aligned} \tag{8}$$

where $[\boldsymbol{c}\times]$ again represents the 3x3 skew symmetric matrix.

Using the matrix determinant lemma, we can also show that $\bar{\mathbf{H}}_{aa} = \mathbf{H}_{aa} - \mathbf{H}_{ap}\mathbf{H}_{pp}^{-1}\mathbf{H}_{pa}$ is invertible since $\mathbf{H}_{aa}^{-1}$ always exists. This can be used to define the change in joint velocities $\Delta\dot{\boldsymbol{q}}_a$ given an actuator impulse: $\Delta\dot{\boldsymbol{q}}_a = \bar{\mathbf{H}}_{aa}^{-1}\boldsymbol{\iota}_a$. Therefore, we can define an equation for $\Delta\boldsymbol{l}$ in terms of $\boldsymbol{\iota}_a$:

$$\Delta\boldsymbol{l} = \boldsymbol{\iota}_0 = \bar{\mathbf{H}}_{0a}\Delta\dot{\boldsymbol{q}}_a = \bar{\mathbf{H}}_{0a}\bar{\mathbf{H}}_{aa}^{-1}\boldsymbol{\iota}_a \tag{9}$$

This also allows us to define the momentum gain matrices $\mathbf{G}_{ma}$ and $\mathbf{G}_{oa}$ in terms of the velocity gain matrices, where $\boldsymbol{G}_m(\boldsymbol{\iota}_a) = \mathbf{G}_{ma}\boldsymbol{\iota}_a$ and $\boldsymbol{G}_o(\boldsymbol{\iota}_a) = \mathbf{G}_{oa}\boldsymbol{\iota}_a$, as:

$$\mathbf{G}_{ma} = \begin{bmatrix}\bar{\boldsymbol{H}}_{xa}\\ \bar{\boldsymbol{H}}_{ya}\end{bmatrix}\bar{\mathbf{H}}_{aa}^{-1} = m\mathbf{G}_{va}\bar{\mathbf{H}}_{aa}^{-1} \tag{10}$$

$$\mathbf{G}_{oa} = [\boldsymbol{c}\times]\bar{\mathbf{H}}_{0a}\bar{\mathbf{H}}_{aa}^{-1} = mc^2\mathbf{G}_{\omega a}\bar{\mathbf{H}}_{aa}^{-1} \tag{11}$$

D. Spatial Gains

Using spatial notation, the centroidal momentum of a system is defined as the aggregated angular and linear momenta of the system's links computed at the system's overall COM [21]. The linear component ($\boldsymbol{l}$) of the centroidal momentum ($\hat{\boldsymbol{h}}_C$) is the linear momentum of the system ($\boldsymbol{l} = m\dot{\boldsymbol{c}}$), while the angular component ($\boldsymbol{k}_C$) is the total angular momentum the system has about its overall COM.

As shown in (5), momentum gains are calculated using only a system's change in linear momentum, $\Delta\boldsymbol{l}$. This is due to the use of a passive rotational contact point, which causes $\Delta\boldsymbol{k}_0 = \mathbf{0}_{3\times1}$ [7]. Therefore, by using the contact point as the reference point, the change in angular momentum about the COM is: $\Delta\boldsymbol{k}_C = \Delta\boldsymbol{k}_0 - \boldsymbol{c}\times\Delta\boldsymbol{l} = -\boldsymbol{c}\times\Delta\boldsymbol{l}$.

This relation is part of the spatial transformation matrix ($\hat{\boldsymbol{X}}_C$) from the contact to the COM, which maps the total system momentum at the contact ($\hat{\boldsymbol{h}}_0$) to the centroidal momentum: $\hat{\boldsymbol{h}}_C = \hat{\boldsymbol{X}}_C^T\hat{\boldsymbol{h}}_0$. Using $\hat{\boldsymbol{X}}_C$, and that $\Delta\boldsymbol{k}_0 = \mathbf{0}_{3\times1}$ due to passive contact, we define spatial gain as $\boldsymbol{G}_h = \Delta\hat{\boldsymbol{h}}_C$:

$$\boldsymbol{G}_h = \hat{\boldsymbol{X}}_C^T\Delta\hat{\boldsymbol{h}}_0 = \begin{bmatrix}\boldsymbol{I}_{3\times3} & -[\boldsymbol{c}\times]\\ \mathbf{0}_{3\times3} & \boldsymbol{I}_{3\times3}\end{bmatrix}\begin{bmatrix}\mathbf{0}_{3\times1}\\ \Delta\boldsymbol{l}\end{bmatrix} = \begin{bmatrix}\boldsymbol{G}_k\\ \boldsymbol{G}_l\end{bmatrix} \tag{12}$$

where $\boldsymbol{G}_k = -\boldsymbol{c}\times\Delta\boldsymbol{l} = -mc^2\Delta\dot{\boldsymbol{\phi}}$ and $\boldsymbol{G}_l = \Delta\boldsymbol{l} = m\Delta\dot{\boldsymbol{c}}$.

If we assume $\|\Delta\dot{\boldsymbol{q}}_a\| = 1$ or $\|\boldsymbol{\iota}_a\| = 1$, we can define these gains in terms of $\boldsymbol{G}_\omega$ and $\boldsymbol{G}_v$ or $\boldsymbol{G}_o$ and $\boldsymbol{G}_m$, respectively:

$$\begin{aligned}\boldsymbol{G}_k(\Delta\dot{\boldsymbol{q}}_a) &= -mc^2\boldsymbol{G}_\omega & \boldsymbol{G}_k(\boldsymbol{\iota}_a) &= -\boldsymbol{G}_o\\ \boldsymbol{G}_l(\Delta\dot{\boldsymbol{q}}_a) &= m\begin{bmatrix}\boldsymbol{G}_v\\ G_g(\Delta\dot{\boldsymbol{q}}_a)\end{bmatrix} & \boldsymbol{G}_l(\boldsymbol{\iota}_a) &= \begin{bmatrix}\boldsymbol{G}_m\\ G_g(\boldsymbol{\iota}_a)\end{bmatrix}\end{aligned} \tag{13}$$

We can use these equations to define gain matrices for the new gains $\boldsymbol{G}_l(\Delta\dot{\boldsymbol{q}}_a)$ and $\boldsymbol{G}_k(\Delta\dot{\boldsymbol{q}}_a)$ as:

$$\mathbf{G}_{la}(\Delta\dot{\boldsymbol{q}}_a) = \bar{\mathbf{H}}_{0a} \qquad \mathbf{G}_{ka}(\Delta\dot{\boldsymbol{q}}_a) = -[\boldsymbol{c}\times]\bar{\mathbf{H}}_{0a} \tag{14}$$

For the momentum equivalents, we post-multiply these gain matrices by $\bar{\mathbf{H}}_{aa}^{-1}$ [7]. Combining these, we can also define the gain matrix $\mathbf{G}_{ha}(\Delta\dot{\boldsymbol{q}}_a)$ in terms of $\bar{\mathbf{H}}_{0a}$ (and as before, $\mathbf{G}_{ha}(\boldsymbol{\iota}_a) = \mathbf{G}_{ha}(\Delta\dot{\boldsymbol{q}}_a)\bar{\mathbf{H}}_{aa}^{-1}$):

$$\boldsymbol{G}_h(\Delta\dot{\boldsymbol{q}}_a) = \begin{bmatrix}-[\boldsymbol{c}\times]\\ \mathbf{I}_{3\times3}\end{bmatrix}\bar{\mathbf{H}}_{0a}\Delta\dot{\boldsymbol{q}}_a = \mathbf{G}_{ha}(\Delta\dot{\boldsymbol{q}}_a)\Delta\dot{\boldsymbol{q}}_a \tag{15}$$

For more details on the gains and their application in the optimization of planar balancing systems, see [6]–[8].

III. Generalized Gain

We now introduce a generalized gain equation, which can be used to calculate any of these gains.

Building on the spatial gain formulation, we define the generalized gain $\boldsymbol{G}(\boldsymbol{u}_a) = \mathbf{G}_a\boldsymbol{u}_a$ for a given system (with $\mathbf{G}_a$ and $\boldsymbol{u}_a$ the generalized gain matrix and input vector, respectively) as

$$\boldsymbol{G} = \mathbf{S}_G\boldsymbol{G}_h(\Delta\dot{\boldsymbol{q}}_a) \qquad \text{s.t. } \|\boldsymbol{u}_a\| = \|\mathbf{S}_a\Delta\dot{\boldsymbol{q}}_a\| = 1 \tag{16}$$

where $\mathbf{S}_G$ is an $n_G \times 6$ gain selection and scaling matrix and $\mathbf{S}_a$ is an $n_a \times n_a$ actuator scaling matrix (with n_G the desired gain vector length and n_a the number of actuated joints). This generalized gain can be used to formulate all of the gains summarized in Section II (from [6], [7]).

Using (15), the generalized gain matrix is defined as

$$\mathbf{G}_a = \mathbf{S}_G\mathbf{G}_{ha}(\Delta\dot{\boldsymbol{q}}_a)\mathbf{S}_a^{-1} \tag{17}$$

In general, the matrix $\mathbf{S}_G$ can be used to both scale each of the computed gains and select which gains are of interest. When computing velocity gains, the generalized input vector $\boldsymbol{u}_a$ is equal to $\Delta\dot{\boldsymbol{q}}_a$, so we set the actuator scaling matrix to $\mathbf{S}_a = \mathbf{I}_{n_a\times n_a}$. For momentum gains, we set the actuator scaling matrix to $\mathbf{S}_a = \bar{\mathbf{H}}_{aa}$ based on the definition $\boldsymbol{\iota}_a = \bar{\mathbf{H}}_{aa}\Delta\dot{\boldsymbol{q}}_a$ from Section II-C. As shown in (17), this leads to the familiar post-multiplication of velocity gain matrices by $\bar{\mathbf{H}}_{aa}^{-1}$ to become momentum gain matrices.

The scaling factors and selection matrices required to formulate each of the gains from Section II are shown in Table I. It also shows the key differences between velocity and momentum gains, as initially discussed in [7]:

- The velocity gains include a division by m, the total mass, and (for the angular portion) by the square of c, the distance between the contact and the COM.
- The momentum gains include $\bar{\mathbf{H}}_{aa}$, which defines the relationship between the change in joint velocities $\Delta\dot{\boldsymbol{q}}_a$ and the impulse $\boldsymbol{\iota}_a$ that causes that change.

Based on these differences, Featherstone's conclusion that there was no objective reason to use momentum gains after defining them for the 2-link planar system in [6] are justified: The mechanism in [6] has only one actuated joint and fixed link lengths and inertias, which would cause the scaling matrices to all simplify to constant positive scalar values.

However, it should be evident based on Table I that in any other case the momentum gains provide additional useful and different information about the system compared to the velocity gains. This is primarily due to the consideration of inertial loading on the actuators via k_G and $\mathbf{S}_a$.

TABLE I

GENERALIZED GAIN FORMULATIONS FOR 2D, 3D, AND SPATIAL GAINS

For these gains, the matrix $\mathbf{S}_G$ can be defined as the product of a scaling factor k_G and a selection matrix $\mathbf{I}_G$: $\mathbf{S}_G = k_G\mathbf{I}_G$. To concisely define $\mathbf{I}_G$, we define $\boldsymbol{e}_i$ as the ith row of the 6×6 identity matrix $\mathbf{I}_{6\times6}$. With a minor abuse of notation, we write the $n_a \times n_a$ identity matrix as $\mathbf{I}_{a\times a}$. For these gains, we can rewrite the generalized gain equation as:

$$\boldsymbol{G} = k_G\mathbf{I}_G \begin{bmatrix} -[\boldsymbol{c}\times] \\ \mathbf{I}_{3\times3} \end{bmatrix} \bar{\mathbf{H}}_{0a}\mathbf{S}_a^{-1}\boldsymbol{u}_a \quad \text{s.t. } \|\boldsymbol{u}_a\| = \|\mathbf{S}_a\Delta\dot{\boldsymbol{q}}_a\| = 1$$

2D, 3D, and Spatial Gains	k_G	$\mathbf{I}_G$	$\mathbf{S}_a$
Spatial Velocity Gain: $\boldsymbol{G}_h(\Delta\dot{\boldsymbol{q}}_a)$	1	$\mathbf{I}_{6\times6}$	$\mathbf{I}_{a\times a}$
3D Angular Velocity Gain: $\boldsymbol{G}_\omega(\Delta\dot{\boldsymbol{q}}_a)$	$\frac{-1}{mc^2}$	$\begin{bmatrix}\boldsymbol{e}_1\\ \boldsymbol{e}_2\\ \boldsymbol{e}_3\end{bmatrix}$	
2D Angular Velocity Gain: $G_\omega(\Delta\dot{\boldsymbol{q}}_a)$		$\boldsymbol{e}_3$	
3D Linear Velocity Gain: $\boldsymbol{G}_v(\Delta\dot{\boldsymbol{q}}_a)$	$\frac{1}{m}$	$\begin{bmatrix}\boldsymbol{e}_4\\ \boldsymbol{e}_5\end{bmatrix}$	
2D Linear Velocity Gain: $G_v(\Delta\dot{\boldsymbol{q}}_a)$		$\boldsymbol{e}_4$	
Spatial Momentum Gain: $\boldsymbol{G}_h(\boldsymbol{\iota}_a)$	1	$\mathbf{I}_{6\times6}$	$\bar{\mathbf{H}}_{aa}$
3D Angular Momentum Gain: $\boldsymbol{G}_o(\boldsymbol{\iota}_a)$	-1	$\begin{bmatrix}\boldsymbol{e}_1\\ \boldsymbol{e}_2\\ \boldsymbol{e}_3\end{bmatrix}$	
2D Angular Momentum Gain: $G_o(\boldsymbol{\iota}_a)$		$\boldsymbol{e}_3$	
3D Linear Momentum Gain: $\boldsymbol{G}_m(\boldsymbol{\iota}_a)$	1	$\begin{bmatrix}\boldsymbol{e}_4\\ \boldsymbol{e}_5\end{bmatrix}$	
2D Linear Momentum Gain: $G_m(\boldsymbol{\iota}_a)$		$\boldsymbol{e}_4$	

IV. GENERALIZED OPTIMIZATION FRAMEWORK

We now develop a framework which optimizes the gains defined above to design bipeds and other balancing mechanisms. Our framework [8] requires five main elements:

- A *model*, defining the parameterized mechanism (including the number of links, joint details, etc.);
- The modifiable parameters $\boldsymbol{x}$ of the model (e.g., link mass, length, COM), with their allowable upper and lower bounds ($\boldsymbol{x}_{min}$ and $\boldsymbol{x}_{max}$, can be $\pm\infty$ if desired);
- A parameter map $\mathbf{X}$, which dictates how to assign a given set of parameters $\boldsymbol{x}$ to the model;
- A set of key poses $\mathbf{Q} = \{\boldsymbol{q}_1, \boldsymbol{q}_2, \dots\}$ in the model's configuration space (including the passive joint); and
- An objective function $J(\boldsymbol{x})$ which quantifies a model's ability to achieve a desired behavior for a given $\boldsymbol{x}$.

Once these five elements have been selected, a global optimization is used to find the optimal parameterization:

$$\max_{\boldsymbol{x}} J(\boldsymbol{x}), \quad \text{s.t.} \quad \boldsymbol{x}_{min} \le \boldsymbol{x} \le \boldsymbol{x}_{max} \tag{18}$$

The objective function in [8] was the mean of the pose-specific objective function $J(\boldsymbol{q}, \boldsymbol{x})$ across all n_q key poses:

$$J(\boldsymbol{x}) = \frac{1}{n_q}\sum_{i=1}^{n_q} J(\boldsymbol{q}_i, \boldsymbol{x}) \qquad \forall \boldsymbol{q}_i \in \mathbf{Q} \tag{19}$$

In [7], pose-specific objective functions were defined for each planar gain, quantifying the model's balancing ability for each $(\boldsymbol{q}, \boldsymbol{x})$ pair as the maximum magnitude each gain could achieve for the given pair (where $J_* = J_*(\boldsymbol{q}, \boldsymbol{x})$):

$$\begin{aligned} J_* &= \max_{\Delta\dot{\boldsymbol{q}}_a} |\boldsymbol{G}_*(\Delta\dot{\boldsymbol{q}}_a)| = \|\mathbf{G}_{*a}\| \quad \text{s.t. } \|\Delta\dot{\boldsymbol{q}}_a\| = 1 \\ J_* &= \max_{\boldsymbol{\iota}_a} |\boldsymbol{G}_*(\boldsymbol{\iota}_a)| = \|\mathbf{G}_{*a}\| \quad \text{s.t. } \|\boldsymbol{\iota}_a\| = 1 \end{aligned} \tag{20}$$

These objective formulations enable the design of parameterized mechanisms without a controller or trajectory, as the gains are a function only of the physical properties of the system in a given configuration. Therefore, the framework is able to determine and improve a system's fundamental physical limits for a desired behavior (typically gait or balance[4]) independent of the controller.

We will now define an objective function to optimize mechanism design using the generalized gain equations from above, building on the approach initially proposed in [8]. We then augment this generalized objective function with weighting matrices to enable the application of domain knowledge to guide the optimization.

The purpose of this novel objective function is to guide the automated optimal design of a mechanism by quantifying its ability to move its COM throughout a given subset of the mechanism's configuration space, without defining or generating an associated controller or trajectory.

A. Generalized Objective Function

We wish to automatically generate an optimal mechanism by maximizing one or more of the gains defined in Section III. When working in 3D, the gains are no longer scalars but vectors. Similarly, if optimization over multiple gains is desired (in 2D or 3D), the overall gain is also a vector. In light of this, a method for choosing what value to optimize as the scalar representation of the overall gain is required.

Therefore, we define the general pose-specific objective function (with the assumption that $\|\boldsymbol{u}_a\| = 1$) as

$$J(\boldsymbol{q}, \boldsymbol{x}) = \max_{\boldsymbol{u}_a} \|\boldsymbol{G}(\boldsymbol{u}_a)\| = \max_{\boldsymbol{u}_a} \|\mathbf{G}_a\boldsymbol{u}_a\| = \|\mathbf{G}_a\| \tag{21}$$

where $\|\mathbf{G}_a\|$ represents the induced matrix norm of $\mathbf{G}_a$.

Choosing which gain(s) and norm(s) to use in the objective function to achieve the desired outcome is a critical step in successfully applying the optimization framework. Here, we considered three different types of high-level goals:

- Maximizing one particular direction of the selected gain for each configuration, with the specific direction either chosen a priori (e.g., sagittal motion) or automatically determined using an ∞-norm on the gain matrix.
- Maximizing the selected gain based on the use of only a single joint in each configuration, with the specific joint either chosen a priori (e.g., ankle pitch) or automatically determined using a 1-norm on the gain matrix.
- Maximizing the largest possible gain in any included direction for each configuration, with the direction determined using a 2-norm on the gain matrix.

[4]Here, we assume that the angular momentum about the COM is negligible or regulated, so balance is only concerned with the COM motion.

Using the first type of goal with a direction chosen a priori effectively results in projecting the 3D system into 2D, where the gain is a scalar and the planar formulation of the objective function from [7] can be used. As an example, we can set the scaling and selection matrices as defined in Table I to duplicate the objective functions defined in (20) and apply 2-norms to reproduce the optimization functions from [7].

For the second goal, which focuses on a specific joint, the formulation of the generalized gain will result in a scalar quantification of how well the system can balance using only that joint. For a joint chosen a priori, this scalar gain is a metric for how well that specific joint can balance the system with the given parameters. For automatically chosen joints, it can also be used to define which joint(s) to use for balance in each region of the robot's configuration space.

For the final goal, which attempts to maximize the overall gain for each configuration, the result is comparable to the ellipses and ellipsoids generated by the (dynamic) COM manipulability metrics defined in [1]–[3].

Although the results of these metrics (both generalized gain and dynamic COM manipulability) can be applied directly to the optimization of a mechanism, their real flexibility and power are revealed when combined with weighting matrices to incorporate domain knowledge into the optimization. For example, combinations of weights can be used to account for scaling issues, differences in units, joint limits (on position, torque, etc.), and even the relative importance of the gain directions and/or the inputs.

To augment the objective function with this kind of expert domain knowledge, weights can be applied to the gain matrix and input vector by using weighted matrix norms in place of the standard induced norms. To this end, we define the weighted general pose-specific objective function (with $J_W = J_W(\boldsymbol{q}, \boldsymbol{x})$ and symmetric positive definite weights) as

$$\begin{aligned} J_W &= \max_{\boldsymbol{u}_a} \|\mathbf{G}_a \boldsymbol{u}_a\|_{\mathbf{W}_G} && \text{s.t. } \|\boldsymbol{u}_a\|_{\mathbf{W}_a} = 1 \\ &= \max_{\boldsymbol{u}_a} \|\mathbf{W}_G \mathbf{G}_a \boldsymbol{u}_a\| && \text{s.t. } \|\mathbf{W}_a \boldsymbol{u}_a\| = 1 \\ &= \max_{\boldsymbol{v}_a} \|\mathbf{W}_G \mathbf{G}_a \mathbf{W}_a^{-1} \boldsymbol{v}_a\| && \text{s.t. } \|\boldsymbol{v}_a\| = 1 \\ &= \|\mathbf{W}_G \mathbf{G}_a \mathbf{W}_a^{-1}\| \\ &= \|\mathbf{G}_a\|_{\mathbf{W}_G, \mathbf{W}_a} \end{aligned} \tag{22}$$

where $\mathbf{W}_G$ and $\mathbf{W}_a$ are the gain and actuator weights, respectively, and the weighted vector norm $\|\cdot\|_A = \|A \cdot\|$ induces the weighted matrix norm $\|\cdot\|_{A,B} = \|A \cdot B^{-1}\|$.

V. 3D 5-Link Biped Model

To validate the general pose-specific objective functions defined in (21) and (22) and show the effects that the different norms and weights have on the resulting parameterization of the model, we apply them to a 3D 5-link biped (see Figure 2). This biped has a passive spherical contact (3 DOF), universal hip joints (2 DOF) separated by a fixed offset[5], and a rotary knee joint (1 DOF) in the swing leg.

[5]Although the relative width of the hips could be used in the optimization, for this work it has been fixed at 20% of the biped's total length.

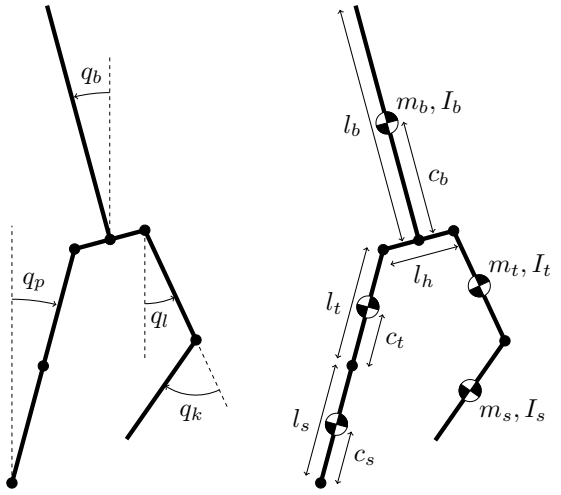

(a) Joint Labels (b) Parameters

Fig. 2. Diagrams of the 3D 5-link biped model. In (a), passive rotations about the contact point q_p, body rotations q_b, and swing leg rotations q_l are all measured relative to a vertical axis, while swing knee rotation q_k is measured relative to a straight leg. In (b), the link parameters are the mass m_i, length l_i, COM c_i, and inertia $I_i = m_i r_i^2$, where the index i is replaced with b, t, or s for the body, thigh, and shank links, respectively. The width of the hips (l_h) has been fixed at 20% of the total length l.

TABLE II
PARAMETER DEFINITIONS FOR 5-LINK BIPED

Parameter	Equation	Min	Max
Body Link Mass	m_b/m	1/2	3/4
Body Link Length	l_b/l	1/4	1/2
Thigh Link Mass	m_t/m_l	1/4	3/4
Thigh Link Length	l_t/l_l	1/3	2/3
All Link COMs	c_i/l_i	1/4	3/4
All Link Inertias	r_i/l_i	0	2/3

Similar to the parameterization of the 2D 5-link biped in [8], here we use a minimal representation of mass and distance ratios based on the four link parameters defined in Figure 2b (as shown in Table II). Note that for this model we have included the inertia of the links in the parameterization via the radius of gyration r_i about the link's parent joint.

We assume that the system has identical, symmetric legs and use the indices b, s and t to indicate the body, shank and thigh links, respectively. The total mass and length of the biped are defined as $m = m_b + 2m_l$ and $l = l_b + l_l$, respectively, where the mass and length of each leg is defined as $m_l = m_s + m_t$ and $l_l = l_s + l_t$, respectively.

When defining the parameterization in Table II, the mass and length of the body link are scaled by the total mass and length of the system, respectively, while the mass and length of the thigh links are scaled by the mass and length of the leg, respectively. This eliminates the need to parameterize the (dependent) mass and length of the shank link.

This parameterization consists of 10 independent parameters, which can be satisfied strictly using lower and upper bounds: two mass ratios, two length ratios, and the COM and inertia for each of the three independent links.

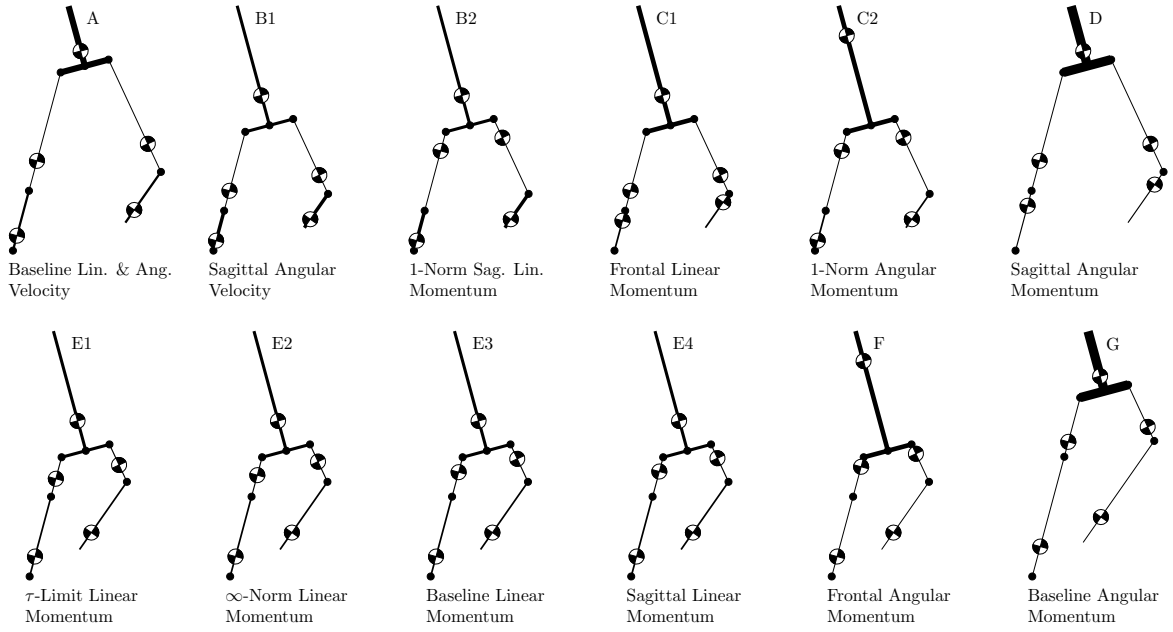

Fig. 3. Diagrams of the models which correspond to the results in Table III. The relative thicknesses of each link denote their relative densities (i.e., short heavy links are thickest, long light links are thinnest). Note that the configuration of the models' joint angles are arbitrary but identical.

The parameter map which applies these parameters to the model, $\mathbf{X}$, assumes $m = 50$ kg and $l = 1$ m to facilitate the calculation of the kinematic and dynamic properties. This means the system's masses, lengths, COMs, and inertias can be defined using real values and applied to the model used in the objective function. However, since the gains are invariant to changes in m and angular gains are invariant to changes in l, the values can be modified with minimal impact.

For this model, key poses have been defined which incorporate a set of typical motion paths within the configuration space of the biped. To generate these key poses, a set of joint ranges has been chosen to approximate the required motions in the swing phase of a standard walking gait, where the swing leg starts on the ground behind the stance leg and finishes in the same pose but with the leg positions switched.

In this type of gait, the stance knee is fully extended for the duration of the stance phase following the results of [22], which showed that optimal periodic gaits for simple bipeds always involve pendular motion in the stance phase, due to the elimination of work by acting as an inverted pendulum.

The considered motion subspace in the biped's configuration space is defined by the following joint angle ranges (which, other than q_k, are all relative to a vertical axis):

$$\begin{aligned} -\pi/6 \leq \quad & q_{px} \quad \leq \pi/6 \\ -\pi/18 \leq \quad & q_{py} \quad \leq \pi/9 \\ -\pi/12 \leq \quad & q_{bx} \quad \leq \pi/12 \\ -\pi/18 \leq \quad & q_{by} \quad \leq \pi/18 \\ -\pi/3 \leq \quad & q_{lx} \quad \leq \pi/3 \\ -\pi/9 \leq \quad & q_{ly} \quad \leq \pi/18 \\ 0 \leq \quad & q_k \quad \leq \pi/3 \end{aligned} \tag{23}$$

TABLE III
GAIN OPTIMIZATION PARAMETERIZATION RESULTS [6]

Label & Main Gain	$\frac{m_b}{m}$	$\frac{l_b}{l}$	$\frac{m_t}{m_l}$	$\frac{l_t}{l_l}$	$\frac{c_b}{l_b}$	$\frac{c_t}{l_t}$	$\frac{c_s}{l_s}$
A: Baseline Velocity	1/2	1/4	1/4	2/3	1/4	1/4	1/4
B1: Sagittal Ang. Vel.	1/2	1/2	1/4	2/3	1/4	1/4	1/4
B2: 1-Norm S. Lin. Mom.						3/4	
C1: Frontal Lin. Mom.	3/4	1/2	1/4	2/3	1/4	1/4	3/4
C2: 1-Norm Ang. Mom.					3/4	3/4	1/4
D: Sagittal Ang. Mom.	3/4	1/4	1/4	2/3	1/4	1/4	3/4
E1: τ-Limit Lin. Mom.	1/2	1/2	1/4	1/3	1/4	.450	1/4
E2: ∞-Norm Lin. Mom.						.540	
E3: Baseline Lin. Mom.						.614	
E4: Sagittal Lin. Mom.						.631	
F: Frontal Ang. Mom.	3/4	1/2	1/4	1/3	3/4	3/4	1/4
G: Baseline Ang. Mom.	3/4	1/4	1/4	1/3	1/4	1/4	1/4

Next, we compare the results of optimizing the parameterized model across this range of motions for the frontal (x), sagittal (y), and combined horizontal (xy) gains using:

- Unweighted 2-norms on the xy gains;
- Unweighted 2-norms on the x and y gains;
- Unweighted ∞-norms on the xy gains;
- Gain-weighted 2-norms on the xy gains;
- Unweighted 1-norms on the x, y, and xy gains; and
- Input-weighted 2-norms on the xy gains.

[6]Note that we have left out the r_i/l_i parameters in this table, as the link inertias were optimized to 0 for every set of results we generated in this work. In a physical robot this is not realistic, but for a model like this it is feasible since we can add inertia back to the links via the addition and subtraction of virtual masses at the joints (see [6] for details).

VI. RESULTS

The resulting optimized parameter sets are summarized in Figure 3 and Table III, where duplicates have been combined under a single label wherever possible. In cases where the only difference between two (or more) optimized parameter sets are the locations of their link COMs, a numbered label is used to distinguish between the lettered sets.

We summarize our high-level observations below:

(1) In general, optimizing a mechanical design for a particular gain will result in a better performing system than any heuristically generated design or even an optimal parameter set from another family of mechanisms. For example, based on the results in [8] we might assume that the mechanism with the best overall balance performance would be parameter set F (which has the same parameters as the optimal 2D 5-link biped as [8]). However, optimizing for the overall horizontal angular momentum gain (and by extension the 3D balance performance) leads to model G, which has very different body ratios and COM locations.

(2) The design generated differs depending on the chosen objective function, with trade-offs between mobility in one direction vs another. This means that a mechanism which is optimized in one direction is typically poor in the other direction. However, based on the numerical results in Table IV, we can see that in some cases a slight reduction in an optimal gain can dramatically increase the gain in the perpendicular direction. See Subsection VI-B for specific examples of these direction-dependent trade-offs.

(3) Using velocity gain(s) results in different mechanisms compared to using momentum gain(s), and each momentum gain objective also results in a different mechanism. The results in Table IV illustrate that most of the velocity gain objectives result in the same parameter set as they do not take into consideration the additional inertial information used to generate momentum gains. In addition, every single optimized momentum gain objective results in a different parameter set, providing evidence that momentum gain objectives lead to quantifiably different designs even for the reduced set of parameters used in this work.

(4) Further, it is important to consider that gains are pose-dependent and will change throughout a given motion and/or configuration space. In Subsection VI-G we will illustrate how the gains changing throughout a given motion will have an effect on the optimization. Here we have used gain ellipses to give a comparable measure to the ground-projected dynamic COM manipulability from [3].

(5) One final general observation about the results in Table IV is that there are families of parameter sets that are good or bad at different types of motions (i.e., have different levels of gain for different types of gains). For example, models A, B1, B2, and E1-4 all have good general angular velocity gains, which leads directly to good balance performance for systems where the inertia is negligible. However, once inertia is taken into account (i.e., in the angular momentum gains) we see that the models with a higher overall COM (C2, F, and G) replace B1, B2, and E1-4 as the peak performers.

A. Baseline: Unweighted 2-Norms

First, we generated a set of baseline results by conducting optimizations using the horizontal components of the four different gains based on the matrix 2-norm with both weighting matrices set to appropriately sized identity matrices.

As shown in Table IV, the baseline results for the linear and angular horizontal velocity gain optimizations both correspond to model A in Figure 3 and Table III. However, the linear and angular momentum gain optimizations resulted in very different parameter sets: E3 and G, respectively.

Compared to the velocity gain results of model A, the linear momentum gain results in E3 maintain the division of mass between the links but the COMs of the thighs shift towards the hips and the relative link lengths change, with the body and shank links growing to maximum length and the thighs shrinking to their minimum.

For the angular momentum gain results in G, there are only two changes from model A: the mass of the body increases to its maximum (lowering the relative mass in the leg links) while the long shanks and short thighs appear again, although this time with no change in the COMs of any link.

These results echo those in [7], where optimizing for linear momentum gain caused a shift of mass closer to the hips while optimizing for angular momentum gain typically led to most of the mass moving further away from the contact.

Intuitively, having heavy "feet" and long legs will result in larger velocity gains, where small hip velocities can produce large COM motions. Since momentum gains include inertial information, they are increased by shifting mass away from the feet towards the hips and body as this reduces the relative torques required to move the COM.

B. A Priori Direction Selection: Frontal and Saggital

To determine how many of the differences between the 2D and 3D 5-link biped results are due to rotating in multiple planes, we also ran optimizations to determine the parameters which would result in the maximum gain in each of the horizontal directions separately. Other than selecting which gain was included in the objective, these results used the same formulation as the baseline optimizations.

As shown in Table IV, the optimal frontal (x) and saggital (y) linear velocity gain parameter sets and the optimal frontal angular velocity gain parameter set are all model A, the same as the baseline velocity gain optimizations. However, the optimal sagittal angular velocity gain parameter set is B1, where the relative length of the body increases to half the model's length (from $1/4$ the length in model A).

When optimizing for momentum gains, differences between the frontal and saggital results emerge when they are optimized independently. These differences can be quantitatively and qualitatively analyzed by comparing the four different parameter sets generated by these optimizations (corresponding to models C1, D, E4, and F).

The main observation here is that the baseline horizontal momentum gain optimization results (E3 and G) are each dominated by motions in a different direction:

TABLE IV

OBJECTIVE FUNCTION VALUES FOR EACH OPTIMIZED PARAMETER SET

Each of the numerical entries in this table represents the value of the global objective function $J(\boldsymbol{x})$, as defined in (19): the mean of the given pose-specific objective function $J(\boldsymbol{q}, \boldsymbol{x})$ evaluated across the set of n_q poses $\boldsymbol{q} \in \mathbf{Q}$ covering the motion subspace defined in (23) for the given parameter set $\boldsymbol{x}$. When defining these objective functions, the subscripts on the gain matrix or vector indicate which gain is being optimized while the subscript on the norm indicates which type of norm is being applied. Note that in this section, and by extension this table, we are only optimizing for the horizontal components of the gains so the angular gains do not include a vertical component.

	Parameter Set ($\boldsymbol{x}$)											
$J(\boldsymbol{q}, \boldsymbol{x})$	**A**	**B1**	**B2**	**C1**	**C2**	**D**	**E1**	**E2**	**E3**	**E4**	**F**	**G**
$\|\mathbf{G}_{va}\|_2$	0.1956	0.1346	0.1237	0.06235	0.06084	0.08505	0.1162	0.1154	0.1147	0.1146	0.05755	0.09023
$\|\mathbf{G}_{\omega a}\|_2$	0.2449	0.2227	0.2007	0.08022	0.07628	0.08483	0.1823	0.1808	0.1797	0.1795	0.07216	0.09339
$\|\mathbf{G}_{ma}\|_2$	43.87	36.94	37.49	28.43	36.36	28.90	42.64	43.64	43.91	43.90	41.75	41.45
$\|\mathbf{G}_{oa}\|_2$	21.92	13.87	14.52	14.38	23.14	18.69	16.10	16.56	16.83	16.87	25.84	26.01
$\|\boldsymbol{G}_{vxa}\|_2$	0.1175	0.09465	0.08723	0.04587	0.04488	0.05354	0.08186	0.08128	0.08081	0.08071	0.04289	0.05513
$\|\boldsymbol{G}_{vya}\|_2$	0.1376	0.08353	0.07711	0.03899	0.03781	0.06026	0.07387	0.07339	0.07302	0.07294	0.03650	0.06485
$\|\boldsymbol{G}_{\omega xa}\|_2$	0.1837	0.1513	0.1384	0.05753	0.05264	0.06636	0.1316	0.1306	0.1298	0.1297	0.05256	0.07382
$\|\boldsymbol{G}_{\omega ya}\|_2$	0.1352	0.1463	0.1309	0.05277	0.05095	0.04638	0.1165	0.1154	0.1145	0.1143	0.04740	0.04838
$\|\boldsymbol{G}_{mxa}\|_2$	19.50	19.05	7.359	25.59	7.034	24.99	12.65	10.97	9.913	9.720	9.212	17.93
$\|\boldsymbol{G}_{mya}\|_2$	38.11	32.22	37.08	14.78	35.95	14.12	41.34	42.78	43.27	43.29	40.91	36.61
$\|\boldsymbol{G}_{oxa}\|_2$	18.51	11.18	14.42	5.819	23.02	7.033	14.84	15.78	16.31	16.40	25.53	21.24
$\|\boldsymbol{G}_{oya}\|_2$	9.604	7.478	2.139	13.06	3.665	16.60	5.832	4.828	4.081	3.928	5.129	12.43

- The baseline linear momentum results (E3) are dominated by the sagittal dynamics, with only a slight shift in c_t from the sagittal linear momentum results (E4).
- The baseline angular momentum results (G) are dominated by the frontal dynamics: the frontal component of the objective function for set G is almost double the frontal component (and almost $5\times$ for set F).

Comparing the frontal linear momentum results (C1) to the baseline results (E3), most of the mass has shifted to the body link, the thigh link gets as long as possible, and the COM of the leg links shift towards the knee. For the sagittal angular momentum set (D) compared to (G), the thighs get longer and the shank COMs shift towards the knees.

Although the baseline angular momentum results are dominated by the frontal dynamics, the doubling in sagittal angular momentum gain when switching from F to G increases the overall angular momentum gain enough to compensate for the relatively small drop in frontal gain. This also helps to demonstrate a key observation: the overall horizontal gain is always greater than either individual horizontal gain but smaller than their sum, due to the use of induced norms.

It is interesting to note that the non-dominant momentum gain results, corresponding to sets C1 and D, differ only in the relative length of the body link and have the top two values for both the non-dominant momentum gain directions. They are also the two parameter sets with the lowest dominant momentum gains and lowest baseline linear momentum gain, but these differences are almost unnoticeable when looking at the baseline angular momentum gain.

Further, looking at models B2 and C1, where the objective values for the angular momentum gain are separated by less than 1%, the overall performance of the models might appear to be similar. However, looking at sizable differences in the directional angular momentum gains for these models shows that they will actually perform differently in the two given directions. This disparity between the baseline and directional gains justifies the need for weighting and selection when optimizing mechanisms for specific tasks.

C. Automatic Direction Selection: Unweighted ∞-Norms

When the gain needs to be optimized in a single direction but the direction is not known a priori, an ∞-norm can be used on the gain matrix to automatically select the single direction with the highest gain in each configuration.

To verify this, we replace each matrix 2-norm used to generate the baseline results with an ∞-norm. When compared to the results of Sections VI-A and VI-B, this formulation should find a parameter set which is similar to both the baseline results and the dominant a priori results.

Although the velocity gain results for this formulation are identical to the baseline results (see model A), the momentum gain results include some interesting relative changes. Specifically, when using the ∞-norm, the linear momentum gain results (model E2) are similar to both the baseline and sagittal 2-norm results (E3 and E4, respectively), as expected.

However, the COM of the thighs has shifted further down the leg, almost to the halfway point between the hip and knee. This shift is in the opposite direction from the shift between the baseline results and the dominant sagittal a priori results, giving an indication that there are configurations where the frontal component of the gain is a larger contributor to the overall linear momentum gain than the sagittal dynamics.

Similarly, the angular momentum gain results (model G) are the same as the baseline results and shares features with the (dominant) frontal results (model F). This is a strong indication that the sagittal dynamics play a minor but critical role in the overall angular momentum gain formulation.

The information gained from an optimization using ∞-norms could also be used for a mechanism with fixed inertial and kinematic parameters: This optimization would provide insight into which directions the system can control the COM more easily (and by extension, balance and move).

D. Weighted Directions: Gain Weighting Matrix

Unlike the optimizations in Sections VI-B and VI-C, which focus on maximizing the gain due to a single component (manually or automatically determined) of the generalized gain for each configuration, there are often applications where multiple components of the generalized gain are important to consider. This is where the 2-norm is generally used, which will result in maximizing the largest possible gain via a combination of the included gain components.

However, there are cases where one of the gain components may be more critical to the performance of the desired behaviour. In this case, the gain weighting matrix can be used to bias the optimization towards a particular component without removing the others from the formulation entirely.

To demonstrate, we have added two different gain weighting matrices to the baseline formulation. To bias the optimization towards the frontal plane, we used a weighting matrix which emphasizes the gain in the x direction:

$$W_G = W_{Xy} = \begin{bmatrix} 9 & 0 \\ 0 & 1 \end{bmatrix} \tag{24}$$

To bias towards the sagittal plane, we use a weighting matrix which emphasizes the gain in the y direction:

$$W_G = W_{xY} = \begin{bmatrix} 1 & 0 \\ 0 & 9 \end{bmatrix} \tag{25}$$

Comparing the results of these weighted gain optimizations to the a priori direction selection results from Section VI-B, we see that when a given plane is emphasized the results of the weighted optimization are identical to the results from the a priori direction selection when the same plane is selected. For example, when the x component is emphasized over the y component using a gain weighting matrix for this model, the results are the same as if the x direction was chosen a priori (and vice versa).

Scaling the relative values of the weights in the W_G matrix can therefore be used to shift an objective across a continuous subspace of gains, ranging from a complete focus on one direction (as seen in Section VI-B) to the equally weighted contributions from multiple directions used in Section VI-A.

E. Automatic Joint Selection: Unweighted 1-Norms

If a single known joint is to be used to realize balancing behavior, the formulation will reduce to the maximization of the chosen vector norm of a column vector (or a scalar, if only one component of the gain is being used).

However, if the goal of the optimization is to determine which single joint should be used for balancing in any particular configuration, possibly to free up the rest of the system's DOFs for other tasks, then the matrix 1-norm can be used in place of the 2-norm from the formulations of our baseline results. As with the previous optimizations, all velocity gain results were identical to the baseline results.

The linear momentum gain results using the 1-norm are different from any other linear momentum results, with the same parameter set as the frontal angular momentum gains (see model F). The angular momentum gain results (model C2) are closer to the rest of the angular momentum results, although they still differ from the (dominant) frontal angular momentum gain results (F) by switching the relative lengths of the thigh and shank links.

The 1-norm can also be applied to the a priori direction results, assuming the matrix norm is used for the single-row gain vector, to determine which joint contributes the most to the selected component of the gain in each pose. For these optimizations, all of the velocity gain results and two of the four momentum gain results (the non-dominant frontal linear momentum and sagittal angular momentum) were identical to their corresponding a priori results using the 2-norm.

The frontal angular momentum gain results were the same as the angular momentum 1-norm results (model C2), as expected since the angular momentum gain is dominated by the frontal dynamics. However, the sagittal linear momentum gain results (model B2) show a similar leg length switching behavior to what was seen for the angular momentum gain results above, when compared to the baseline and sagittal linear momentum gain results that used the 2-norm (corresponding to models E3 and E4, respectively).

These leg length adjustments when switching from the 2-norm to the 1-norm suggest that if a system would benefit from using only a single joint (or a reduced set of joints) for balancing, that longer links further from the contact will provide more relative gain. Intuitively, this makes sense as it implies that the subset of joints being used for COM motion would require longer lever arms to move distant masses.

An additional key observation here is that, even if a mechanism has already been designed and the inertial and kinematic parameters are fixed, an optimization which uses 1-norms to evaluate the gains over a given configuration space can provide insight into which joint can be used most effectively to balance. If the optimization is run on different areas of the configuration space, this could also be used to map which joint should be used in which regions of the space to maximize the model's COM motion capabilities.

F. Weighted Inputs: Actuator Weighting Matrix

In cases where the joints are not all equivalent (different motors, energy sources, etc.) it is often useful to be able to weight these inputs to provide both an indication of relative importance and to avoid joint limits (e.g., maximum torque). This is also useful when it is desirable that only a subset of

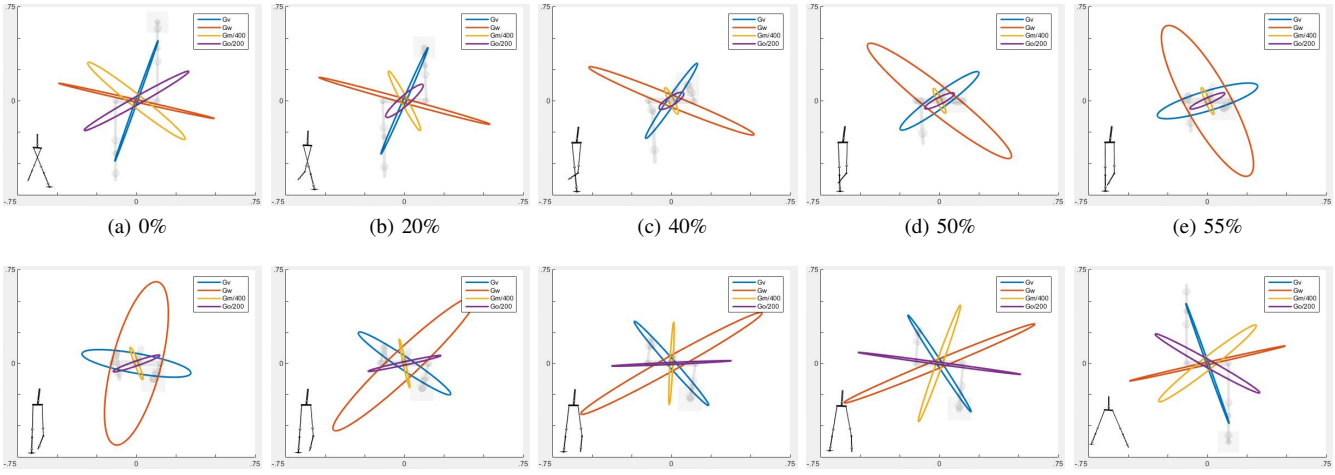

(a) 0% (b) 20% (c) 40% (d) 50% (e) 55%

(f) 60% (g) 65% (h) 70% (i) 75% (j) 100%

Fig. 4. Variations in horizontal gains for a model using parameter set A. The four ellipses in each graph show the magnitudes and directions of the four different baseline horizontal gains for each selected pose, with linear velocity gain in blue, angular velocity gain in orange, scaled linear momentum gain in yellow, and scaled angular momentum gain in purple[8]. The percentage labels on these graphs indicate progress through a complete swing phase (note the gain symmetry between (a) and (j)), while the black stick figure in the lower left of each graph and the underlying gray stick figures show the pose of the model at each point. In this figure, we use gain ellipses based on 2-norms to provide a comparable measure to the ground-projected dynamic COM manipulability of [3]. Please see the video for a better look at how these gains change throughout a step for all of the labeled parameter sets.

joints are to be used for balancing, as in the previous section, which can be given much higher weights than non-balancing joints to drive the solution towards a desirable outcome.

To this end, the generalized objective function also incorporates the ability to apply a weighting matrix to the input vector. As an example, the input vector weights could be similar to those used in [3] for COM manipulability, which correspond to defining either the relative importance of the joint accelerations or the maximum torques.

For this example, we have applied the following input weighting matrix to the input vector, which prioritizes using the hip joints over the knee joints for balance:

$$W_a = 6 \cdot \text{diag}(1,\ 1/9,\ 1/4,\ 1/4,\ 1/9,\ 1) \qquad (26)$$

With this weighting matrix, we can see that the parameter sets either closely or exactly correspond to the automatic direction selection results (using ∞-norms) generated in Section VI-C, corresponding to models A, E1, E2, and G.

G. Variations In Gain due to Pose

In addition to the changes in overall gain due to differences between the parameter sets, it is also critically important to understand how the gains change based on a model's pose. As shown in Figure 4, the magnitudes and directions of each of the gains can vary substantially throughout a given motion, even for a single parameter set (in this case, set A).

For this model, the main reason for these changes in gain direction and magnitude is the motion of the swing leg masses relative to the model's passive contact point, which can cause dramatic shifts in the model's COM and other inertial properties. Since the gains are effectively quantifying the potential of the system to move its COM, longer ellipse axes in Figure 4 correspond to more capacity in the inertial structure of the model to move its COM in that direction.

The gains are also symmetric, since the gains are entirely a function of the static configuration of the joints and the parameters of the model. The symmetry also means fewer gain calculations are required, as the gains can be mirrored from one half of the configuration space to the other.

[8]The scaling of the momentum gains in this figure is purely for the purpose of visual clarity to make all of the gain ellipses a similar size.

VII. Discussion

As introduced in Section V, optimizing a system's gains is equivalent to maximizing the *potential* of that system to be able to move its COM and, by extension, to walk and balance. Applying the optimization framework and generalized objective function defined in this work to a parameterized model will therefore maximize the potential of the given mechanism to effectively move its COM in a region of its configuration space, independent of the controller used or any predefined trajectories within that space.

This optimization provides an upper limit on how well the mechanism can balance and walk using any controller in a range of configurations in the desired motion subspace, avoiding overfitting to a specific controller and/or trajectory. Additionally, the gains are effectively a quantification of the peak COM motion capabilities that could be achieved with a 'perfect' controller, so they could be used as a metric for how close to optimal a controller can move the system's COM.

Currently, humanoid robot performance is compared after the physical mechanism, controller, and trajectories have all been designed. Many of these design choices (especially in the mechanism design) are made through a combination of heuristics and physical fabrication constraints. The optimization approach proposed in this paper also helps to resolve computationally some of the legged robot design trade-offs

that are currently approached heuristically: heavy vs. light feet, long vs. short legs, etc. By providing designers with a quantitative way to compare between different designs (kinematic, inertial, or otherwise), the optimization can even be used to select a reduced region of parameter space within which to heuristically design a system.

To account for real world effects, such as joint limits and energy costs, here weighted norms were used in place of the standard input vector norms (as introduced in [6]). Recent work on dynamic COM manipulability provides some evidence for the benefits of this type of approach, where the input vector has been weighted to account for the torque and acceleration limits of the mechanism's actuators or the relative importance of minimizing joint accelerations [3]. The weighting matrices from [3] were also applied in this work to instantaneous changes in velocity and momentum.

As discussed in [6]–[8], different norms on the actuator input vectors are useful in different scenarios:

- The ∞-norm is an appropriate choice if the most critical issue in the optimization is the effects of joint limits (provided each joint's limits are independent).
- The 1-norm is appropriate if energy consumption is the most critical issue and the energy cost of moving a joint is proportional to its entry in the input vector.
- The 2-norm should be used if the energy cost of moving a joint is proportional to the square of the input vector entry, or if other 2-norm based metrics are being used.

Building on this discussion, we provide general guidelines for choosing the right gain, norm, and weighting matrices given a desired task and mechanism: Typically, as introduced in [8], using an unweighted 2-norm to optimize the angular momentum gain will generate similar results to the standard cost of transport for legged locomotion. This is also a good choice for systems that will be using dynamic balance and require consideration of the inertial rotation about their passive support point (e.g., inverted pendulums).

If a very specific COM motion task must be achieved by the mechanism, to the exclusion and/or detriment of any other tasks, then optimizing for a single gain (or subset of gains) which correlates directly to the direction and goals of that task is recommended.

However, when a more general mechanism capable of achieving several different tasks is desired the balance of objective formulation shifts. In this case, all of the gains associated with the various tasks should be included in the objective formulation and a gain weighting matrix can be used to prioritize between them as needed or compensate for differences in scale and/or units. The constraints on the inputs will again dictate the type of norm and the input weighting matrix, although with a general system typically the 2-norm and the identity matrix will be appropriate.

Ideally, the goal would be to increase the gains in directions where stability is lacking to facilitate recovery motions when needed. Note that these gains represent the peak COM motion performance that any controller will be able to achieve for the given model and parameter set.

Therefore, a model with a high gain and a simple controller can potentially achieve the same COM motion performance as an optimal controller on a low-gain model. In other words, similar performance can be achieved with a simple controller running on an optimized mechanism compared to an optimal controller running on the original mechanism.

Due to the strong dependence of these (and other) gains on the configuration and parameters of the model, there is not yet a clear and effective method of manually designing a high-gain system. This is the key motivating factor behind the development of the generalized optimization framework in Section IV and the validation of the components of the framework that has been described in this section.

VIII. Conclusion

In this paper, we have formulated a generalized gain for walking and balancing mechanisms that quantifies their COM motion properties and encapsulates and clarifies the relationship between velocity and momentum gains.

This novel gain formulation provides an easily defined metric for analyzing the COM motion capabilities of any mechanism using passive contact to interact with its environment, which enables simple quantitative comparisons between different mechanisms across the design space.

To this end, the generalized gain formulation was combined with weighted matrix norms to produce a generalized objective function for optimizing the design of parameterized mechanisms. Since these gains are all invariant to a scaling of total mass and the angular gains are invariant to a scaling of total length, entire families of mechanisms can be optimized in one application of the customizable framework.

This generalized objective function provides an additional tool for mechanism designers to automatically explore the design space of their given mechanism, without having to generate simulations, trajectories, or controllers. The gains' invariance to mass and length scaling also means that a smaller, cheaper prototype can be built and tested to evaluate the performance of a full size system.

An existing design with fixed kinematic and inertial parameters can also benefit from the application of a gain-based optimization. For example, using 1-norms to evaluate the system's gains over a given configuration space will provide insights into which joint can be used most effectively to move the COM in each region of its configuration space.

As an example of the benefits of this optimization scheme, the generalized optimization framework was applied to a parameterized 3D 5-link biped using 3 different types of norms and several different weighting schemes.

A. Future Work

Our goal is to develop robust underactuated mechanisms which are inherently easy to balance and move, embedding as much capability into the mechanism itself as possible to enable the use of simple controllers to achieve complex tasks.

One direction for future work is the use of generalized gains in parallel with other suitable objectives for the design of a more complex system. This would benefit from an

examination of the *position gains*, defined briefly in [6] as the integral of velocity gain along a path in configuration space, and the analogous gains found by integrating the momentum gains along a similar configuration space path.

Another direction for future work would be the use of these gains, in tandem with other objective metrics, for the optimized design of more complex 3D systems. An important question is how to effectively compare gains in a mechanism's configuration space. Since the configuration space of typical complex and/or 3D systems are not human-readable in most cases, this work could augment the existing tools available for designing these systems with an understanding of how effectively the mechanism could move its COM.

Finally, instead of using weighted matrix norms as is done in this work, other formulations of a scalar objective from a vector of gains could also be explored in future, such as minimizing the condition number of the gain matrix or maximizing its smallest singular value.

REFERENCES

[1] S. Cotton, P. Fraisse, and A. P. Murray, "On the Manipulability of the Center of Mass of Humanoid Robots: Application to Design," *Proceedings of the ASME 2010 International Design Engineering Technical Conferences & Computers and Information in Engineering Conference*, pp. 1259–1267, 2010.

[2] Y. Gu, C. S. Lee, and B. Yao, "Feasible Center of Mass Dynamic Manipulability of humanoid robots," *Proceedings - IEEE International Conference on Robotics and Automation*, vol. 2015-June, no. June, pp. 5082–5087, 2015.

[3] M. Azad, J. Babic, and M. Mistry, "Dynamic manipulability of the center of mass: A tool to study, analyse and measure physical ability of robots," in *IEEE International Conference on Robotics and Automation (ICRA)*, 2017, pp. 3484–3490.

[4] R. Featherstone, "Analysis and Design of Planar Self-Balancing Double-Pendulum Robots," in *RoManSy 19 Robot Design, Dynamics and Control*, V. Padios, P. Bidaud, and O. Khatib, Eds. Springer Vienna, 2013, pp. 259–266.

[5] R. Featherstone, "Quantitative Measures of a Robots Ability to Balance," in *Robotics Science and Systems*, 2015.

[6] R. Featherstone, "Quantitative measures of a robots physical ability to balance," *The International Journal of Robotics Research*, vol. 35, no. 14, pp. 1681–1696, 2016.

[7] B. J. DeHart and D. Kulić, "Quantifying Balance Capabilities using Momentum Gain," in *IEEE-RAS International Conference on Humanoid Robots (HUMANOIDS)*, 2017, pp. 561–568.

[8] B. J. DeHart and D. Kulić, "Legged Mechanism Design with Momentum Gains," in *IEEE-RAS International Conference on Humanoid Robots (HUMANOIDS)*, 2017, pp. 593–598.

[9] C. Paul and J. C. Bongard, "The Road Less Travelled : Morphology in the Optimization of Biped Robot Locomotion," in *IEEE/RSJ International Conference on Intelligent Robots and Systems (IROS)*, 2001, pp. 226 – 232.

[10] K. Endo, T. Maeno, and H. Kitano, "Co-evolution of Morphology and Walking Pattern of Biped Humanoid Robot using Evolutionary Computation - Evolutionary Designing Method and its Evaluation - ," in *IEEE/RSJ International Conference on Intelligent Robots and Systems (IROS)*, 2003, pp. 340–345.

[11] M. Haberland and S. Kim, "On extracting design principles from biology: I. Method-General answers to high-level design questions for bioinspired robots," *Bioinspiration & Biomimetics*, vol. 10, 2015.

[12] M. Haberland and S. Kim, "On extracting design principles from biology: II. Case studythe effect of knee direction on bipedal robot running efficiency," *Bioinspiration & Biomimetics*, vol. 10, no. 1, p. 016011, 2015.

[13] U. J. Römer, C. Kuhs, M. J. Krause, and A. Fidlin, "Simultaneous optimization of gait and design parameters for bipedal robots," in *IEEE International Conference on Robotics and Automation (ICRA)*, 2016, pp. 1374–1381.

[14] G. Saurel, J. Carpentier, and J.-P. Laumond, "A Simulation Framework for Simultaneous Design and Control of Passive Walkers," in *IEEE International Conference on Simulation, Modeling, and Programming for Autonomous Robots*, 2016, pp. 104–110.

[15] G. Buondonno *et al.*, "Actuator Design of Compliant Walkers via Optimal Control," *Rapport LAAS*, no. 17049, 2017.

[16] E. R. Westervelt, J. W. Grizzle, and D. E. Koditschek, "Hybrid Zero Dynamics of Planar Biped Walkers," *IEEE Transactions on Automatic Control*, vol. 48, no. 1, pp. 42–56, 2003.

[17] F. Romano *et al.*, "The CoDyCo Project achievements and beyond: Towards Human Aware Whole-body Controllers for Physical Human Robot Interaction," *IEEE Robotics and Automation Letters*, vol. 3, no. 1, pp. 516–523, 2018.

[18] M. Azad, "Balancing and Hopping Motion Control Algorithms for an Under-actuated Robot," Ph.D. dissertation, Australian National University, 2014.

[19] M. Azad and R. Featherstone, "Angular momentum based balance controller for an under-actuated planar robot," *Autonomous Robots*, vol. 40, no. 1, pp. 93–107, 2016.

[20] R. Featherstone, "A simple model of balancing in the plane and a simple preview balance controller," *The International Journal of Robotics Research*, vol. 36, no. 13-14, pp. 1489–1507, 2017.

[21] D. E. Orin and A. Goswami, "Centroidal Momentum Matrix of a humanoid robot: Structure and properties," in *IEEE/RSJ International Conference on Intelligent Robots and Systems*, 2008, pp. 653–659.

[22] M. Srinivasan and A. Ruina, "Computer optimization of a minimal biped model discovers walking and running," *Nature*, vol. 439, no. 7072, pp. 72–75, 2006.